Site-Resolved Contributions to the Magnetic-Anisotropy Energy and Complex Spin Structure of Fe/MgO Sandwiches

Ramón Cuadrado,[1,2,3,*] László Oroszlány,[4] András Deák,[5] Thomas A. Ostler,[6,7] Andrea Meo,[1] Roman V. Chepulskii,[8] Dmytro Apalkov,[8] Richard F. L. Evans,[1] László Szunyogh,[5,9] and Roy W. Chantrell[1]

[1]*Department of Physics, University of York, York YO10 5DD, United Kingdom*
[2]*Catalan Institute of Nanoscience and Nanotechnology (ICN2), CSIC and BIST, Campus UAB, Bellaterra, 08193 Barcelona, Spain*
[3]*Universitat Autonoma de Barcelona, 08193 Bellaterra (Cerdanyola del Valles), Spain*
[4]*Department of Physics of Complex Systems, Eötvös University, Pázmány Péter sétány 1/A, H-1117 Budapest, Hungary*
[5]*Department of Theoretical Physics, Budapest University of Technology and Economics, Budafoki út 8, H-1111 Budapest, Hungary*
[6]*Faculty of Arts, Computing, Engineering and Sciences, Sheffield Hallam University, Howard Street, Sheffield, S1 1WB, United Kingdom*
[7]*Department of Physics, Université de Liège, B-4000 Liège, Belgium*
[8]*Samsung Electronics, Semiconductor R and D Center (Grandis), San Jose, California 95134, USA*
[9]*MTA-BME Condensed Matter Research Group, Budapest University of Technology and Economics, Budafoki út 8, H-1111 Budapest, Hungary*

(Received 4 December 2017; revised manuscript received 9 April 2018; published 30 May 2018)

Fe/MgO-based magnetic tunnel junctions are among the most promising candidates for spintronic devices due to their high thermal stability and high tunneling magnetoresistance. Despite its apparent simplicity, the nature of the interactions between the Fe and MgO layers leads to complex finite-size effects and temperature-dependent magnetic properties which must be carefully controlled for practical applications. In this article, we investigate the electronic, structural, and magnetic properties of MgO/Fe/MgO sandwiches using first-principles calculations and atomistic spin modeling based on a fully parametrized spin Hamiltonian. We find a large contribution to the effective interfacial magnetic anisotropy from the two-ion exchange energy. Minimization of the total energy using atomistic simulations shows a surprising spin-spiral ground-state structure at the interface owing to frustrated ferromagnetic and antiferromagnetic interactions, leading to a reduced Curie temperature and strong layerwise temperature dependence of the magnetization. The different temperature dependences of the interface and bulklike layers results in an unexpected nonmonotonic temperature variation of the effective magnetic-anisotropy energy and temperature-induced spin-reorientation transition to an in-plane magnetization at low temperatures. Our results demonstrate the intrinsic physical complexity of the pure Fe/MgO interface and the role of elevated temperatures providing insight when interpreting experimental data of nanoscale magnetic tunnel junctions.

DOI: 10.1103/PhysRevApplied.9.054048

I. INTRODUCTION

The control of perpendicular magnetocrystalline anisotropy (PMCA) at ferromagnetic transition–metal-insulator interfaces is of paramount importance in the manufacture of spintronic devices, such as perpendicular magnetic tunnel junctions [1–3] and tunneling anisotropic magnetoresistive systems [4]. Large PMCA can be achieved by fabricating heterostructures including heavy nonmagnetic elements with large spin-orbit coupling (SOC) [5], such as Co/Pt or Co/Au [6]. It has been shown that this out-of-plane PMCA enhancement at the interface is due to an increase of orbital moment of Co atoms and strong hybridization of the 3*d*-5*d* orbitals between the transition metals and the heavy atoms [6–9]. Recently, it has been demonstrated that other 3*d* transition metal elements show increased PMCA even if their spin-orbit coupling is weak [10–12]. Such is the case of Fe-based thin films at MgO(001) interfaces, where the Fe $d_{z^2}-\mathrm{O}\ p_z$ hybridization at the interfaces results in enhanced PMCA [13].

Using *ab initio* calculations Yavorsky and Mertig [14] have shown the existence of antiferromagnetic Fe/Fe interactions in the Fe plane connected to the MgO. From this, they inferred the intriguing possibility of noncollinear

*ramon.cuadrado@icn2.cat

magnetic structures but did not determine the ground-state spin structure. In addition to the possibility of antiferromagnetic interactions, the ground-state spin configuration will be perturbed due to the complex distance-dependent exchange interactions, which is difficult to quantify in layered systems with broken out-of-plane translational invariance. Spin fluctuations at elevated temperatures, coupled with the effects of any noncollinearity, will naturally lead to complex temperature-dependent behavior of the magnetic properties, including the magnetocrystalline anisotropy energy (MAE).

While there are a large number of applications of magnetic-nonmagnetic interfaces such as generating Skyrmions [15] or as magnetic tunnel junctions [16] in magnetic random-access memories, the physical properties of such interface systems (including Fe/MgO) are not fully understood. At the electronic level there exists a basic understanding of the interface exchange [14] and anisotropy [17], with very little understanding of thermal and long-range magnetic-ordering effects. Detailed understanding of the magnetization dynamics and temperature-dependent magnetic properties, particularly that of the magnetization and anisotropy, require a multiscale approach based on atomistic spin dynamics [18] with *ab initio* parametrization. This is especially important given the localization of the magnetic anisotropy at the interface and the possibility of noncollinear spin structures.

In this article, we use a multiscale approach to model the electronic, structural, and magnetic properties of the Fe/MgO interface in a sandwich geometry. Our results reveal the role of single-ion and two-ion anisotropy contributions, as well as the long-range exchange interactions in the ground-state configurations of two different bcc-Fe thicknesses sandwiched by two MgO(001) regions: $\cdots \mathrm{MgO}/n_{\mathrm{Fe}}\mathrm{Fe}/\mathrm{MgO}\cdots$ ($n_{\mathrm{Fe}} = 4, 8$). We show that the lack of Fe out-of-plane symmetry and dissimilar in-plane lattice constants compared to the Fe bulk have a drastic effect on the magnetic properties at the Fe/MgO interface, leading to an exchange anisotropy which provides a dominant contribution to the total PMCA. Through atomistic simulations we show that the complex interfacial exchange interactions lead to a spiral ground-state spin structure. The temperature dependence of the anisotropy is shown to be nonmonotonic, driven by the different temperature dependences of the single-ion and two-ion anisotropies and leads to a significant reduction in the Curie temperature of the system as observed experimentally.

II. DETAILS OF THE CALCULATIONS

We use the SIESTA software package [19] to obtain the final $\cdots \mathrm{MgO}/n_{\mathrm{Fe}}\mathrm{Fe}/\mathrm{MgO}\cdots$ configurations used in the screened Korringa-Kohn-Rostoker (SKKR) calculations [20] by performing fully ionic conjugate gradient relaxation (see Sec. I of the Supplemental Material [21]). For the calculations we use a high number of MgO planes since the SKKR method requires the system to be considered as an intermediate layer region positioned between two semi-infinite bulk regions. From the fully relaxed geometry, a $9\mathrm{MgO}/n_{\mathrm{Fe}}\mathrm{Fe}/9\mathrm{MgO}$ slice is extracted and embedded into the MgO bulk, resulting in an Fe layer sandwiched between two semi-infinite MgO bulk alloys. The presence of the MgO interface leads to enhanced interfacial magnetic and orbital moments, giving total moments of approximately 2.8 μ_B at the interface compared to approximately 2.3 μ_B in the middle of the sandwich, as detailed in the Supplemental Material.

The layer-resolved exchange [22] and anisotropy contributions we calculate using the SKKR code (see Sec. I of the Supplemental Material for details [21]), allowing for a mapping onto a classical spin Hamiltonian [23,24]

$$\mathcal{H} = -\sum_{i<j} \mathbf{S}_i \mathcal{J}_{ij} \mathbf{S}_j - \sum_i k_i (\mathbf{S}_i \cdot \mathbf{e})^2, \tag{1}$$

where $\mathbf{S}_i$ is a classical unit vector parallel to the magnetization at site i, $\mathcal{J}_{ij}$ is the exchange-interaction tensor between sites i and j, and the last term represents the on-site anisotropy, with the anisotropy constant k_i and $\mathbf{e}$ the easy axis direction. Within the SKKR formalism, the total MAE, defined as the total energy difference between hard and easy magnetization directions, can be resolved into layerwise contributions K_l

$$K = \sum_l K_l = K_{\text{on site}} + K_{\text{two site}}, \tag{2}$$

where $K_{\text{on site}} = \sum_i k_i$ and $K_{\text{two site}}$ is given an exchange anisotropy by the difference in the zz and xx components of the exchange tensor.

$$K_{\text{two site}} = -\sum_{i<j} (J_{ij}^{xx} - J_{ij}^{zz}). \tag{3}$$

III. RESULTS

A. Layered resolved magnetic anisotropy

The layer and site-resolved anisotropy contributions are shown in Fig. 1 for (a) $n_{\mathrm{Fe}} = 4$ and (b) $n_{\mathrm{Fe}} = 8$ layers. The Mg and O atoms make a negligible contribution to the MAE. At the interface, specifically on the first two Fe planes, the on-site values (blue filled squares) present higher values compared to those in the center for any configuration. In addition, these positive values imply that the Fe atoms contribute to the total MAE with an out-of-plane anisotropy. However, as the thickness increases, the on-site anisotropy in the center becomes more complex and for $n_{\mathrm{Fe}} = 8$ the easy axis lies in-plane.

For four Fe planes ($n_{\mathrm{Fe}} = 4$), the on-site contribution to the MAE is four times larger than that of the $n_{\mathrm{Fe}} = 8$ case, which we attribute to the enhanced orbital magnetic moment from the small number of Fe planes in the system.

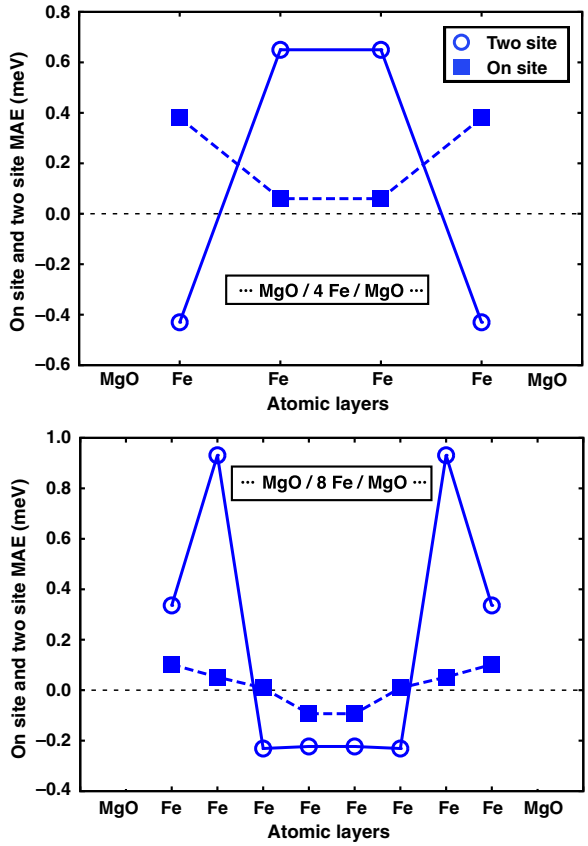

FIG. 1. On-site and two-site MAE contributions for $\cdots \mathrm{MgO}/n_{\mathrm{Fe}}\mathrm{Fe}/\mathrm{MgO}\cdots$ ($n_{\mathrm{Fe}} = 4,\ 8$).

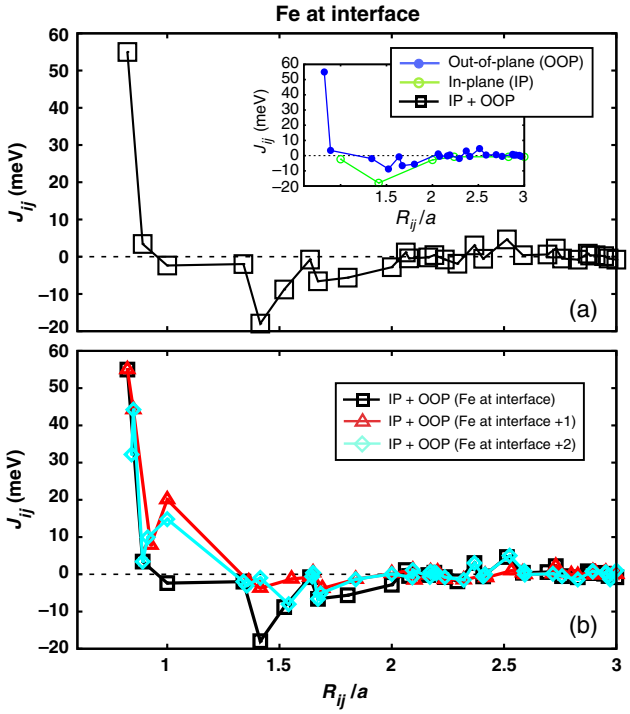

FIG. 2. (a) Fe-Fe isotropic magnetic exchange interactions as a function of the neighbor distances for an Fe atom located at the interface of the $\cdots \mathrm{MgO}/8\mathrm{Fe}/\mathrm{MgO}\cdots$ configuration. The inset shows the intralayer and interlayer isotropic exchange contributions. (b) Fe-Fe isotropic magnetic exchange interactions for Fe at interface (black squares), at interface +1 (red triangles), and at interface +2 (turquoise diamonds). The solid lines are guides for the eye.

The thickness dependence of the two-site anisotropy is more complicated, showing a sign change for the interface layer between $n_{\mathrm{Fe}} = 4$ and $n_{\mathrm{Fe}} = 8$ layers and also the appearance of a preferred in-plane orientation of the magnetization at the center of the $n_{\mathrm{Fe}} = 8$ layer sandwich. In all cases the two-ion contributions to the MAE are seen to be dominant. Because of the different temperature-dependent scalings of single-ion and two-ion anisotropies [25] with the magnetization (m^3 and m^2 at low temperature, respectively) their relative magnitudes determine the overall temperature dependence of the PMCA. Most *ab initio* calculations do not distinguish the origin of the PMCA, only its magnitude and, therefore, simple assumptions for the macroscopic temperature dependence of the anisotropy based on Callen-Callen theory [26] are likely to be erroneous. It is worth mentioning that other theoretical works have been performed in order to gain more insight into the nature of PMCA at Fe/MgO interfaces [17] and at CoFe/MgO interfaces for different compositions [27]. In good agreement with our results (see Fig. 1), both works conclude that the main contributions to the anisotropy energy come from the two ferromagnetic layers closest to the interface. Zhang *et al.* [27] found that the PMCA at $\mathrm{Co}_{1_x}\mathrm{Fe}_x/\mathrm{MgO}$ interfaces strongly depends on the composition of CoFe, decreasing with increasing Co concentration. Moreover, at a certain x value there is a transition from positive to negative MCA. Hallal and co-workers [17] found that, besides the main interfacial contribution, the anisotropy energy propagates into the ferromagnetic bulk, showing an attenuating oscillatory behavior. In the present work (see the entry for $n_{\mathrm{Fe}} = 8$ in Fig. 1) we also clearly observe this oscillatory behavior of the anisotropy energy.

B. Magnetic exchange interactions

In addition to site-resolved anisotropies, we study the effect of the MgO/Fe interface on the interatomic exchange interactions. To aid analysis, we consider the trace of the exchange tensor $J_{ij}^{\mathrm{iso}} = \frac{1}{3}\mathrm{Tr}\mathcal{J}_{ij}$ which forms the dominant part of the exchange energy. The range dependence of the exchange energy for the $n_{\mathrm{Fe}} = 8$ system for different layers is shown in Fig. 2(a). As is commonly observed, the exchange interactions are long ranged and oscillatory in nature but also dominated by interactions with the nearest magnetic moments and decay rapidly with interatomic distance. The leading terms for all layers are ferromagnetic, leading to a general expectation of ferromagnetic ordering as would be expected for Fe. For bulk Fe, the exchange, as

also shown by Yavorsky *et al.* [14]), shows antiferromagnetic contributions with the behavior becoming oscillatory after a couple of lattice spacings. However, in the Fe/MgO interface system, the exchange remains antiferromagnetic for interactions out to a much longer range. To better resolve the origin of the ferromagnetic interactions we have separated the exchange interactions by layer in Fig. 2(b). This separation clearly shows that the large antiferromagnetic interactions in the interface layer occurs between atoms in the same plane. For the smaller $n_{\mathrm{Fe}} = 4$ system, the nearest-neighbor interactions are similar, while the in-plane antiferromagnetic interactions are 40 meV larger, likely leading to a qualitatively different magnetic structure. In general, the isotropic Fe exchange at the interfaces for any n_{Fe} behaves in the same way, i.e., from the third Fe layer the magnetic behavior is similar to any Fe atom within the bulk and the main differences in the magnetic properties arise at the interface.

C. Mesoscopic temperature dependence

While the *ab initio* calculations give information about the nature of the interactions in the system, their complex nature makes it difficult to draw clear conclusions about the macroscopic magnetic properties of the system as the ground state is governed by the balance of the whole set of interactions. The *ab initio* calculated Hamiltonian can then be used to determine the ground-state structure at elevated temperatures through atomistic spin modeling. The calculations utilize the VAMPIRE software package [28,29] considering a $10\ \mathrm{nm} \times 10\ \mathrm{nm} \times 8$ monolayer (ML) system of Heisenberg spins with periodic boundary conditions in the plane. We consider the full exchange tensor of over 2000 interactions per spin, localized anisotropy, and magnetic moments in the simulations. Metropolis and constrained [25] variants of Monte Carlo algorithms are used to determine the ground-state spin configurations in a plane-by-plane manner as well as the Curie temperature and temperature-dependent anisotropy.

A visualization of the final magnetic ground states for $n_{\mathrm{Fe}} = 8$ are shown in Figs. 3(a) and 3(b). In (a) the top plane represents Fe at the MgO interface where a spin-spiral ground state appears due to the frustration between ferromagnetic and antiferromagnetic interactions and the appearance of Dzyaloshinkii-Moriya interactions (DMI) [30,31] at the interface due to broken inversion symmetry. The temperature dependence of the spin-spiral state is discussed in Sec. IV of the Supplemental Material [21]. Interestingly, the orientation of the spiral is at approximately 16.4° to the x axis and the spin spiral is confined to the positive z values ($S_z > 0$). Moving layerwise towards the center of the sandwich, the spin spiral becomes much less prominent and a ferromagnetic ordering dominates, which confirms that the interfacial antiferromagnetic nearest-neighbor interactions and DMI are responsible for the frustrated spin-spiral structure. In fact, such a complex

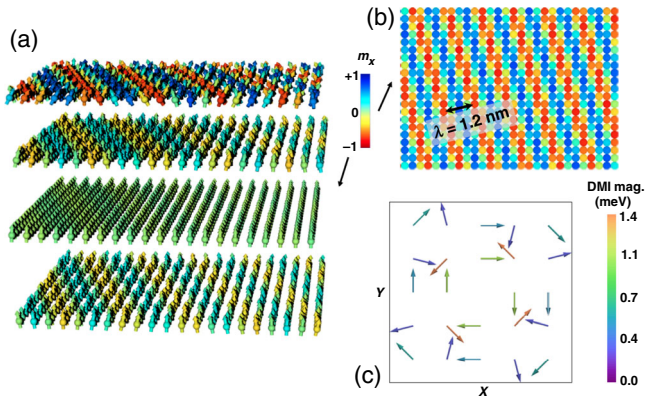

FIG. 3. Perspective (a) and top (b) view of the simulated ground-state spin structure at the n_{Fe}-Fe/MgO interface for $n_{\mathrm{Fe}} = 8$, leading to a near-ferromagnetic state in the center of the sandwich. The coloring indicates the x component of the magnetization (blue for $+x$, red for $-x$, and green for $x = 0$). The atomic moments form a noncollinear configuration with wavelength $\lambda = 1.2$ nm and angle between spins no larger than 45° in the perpendicular direction. (c) Plot of Dzyaloshinsky-Moriya interactions (DMI), which lay in the x-y plane solely, for the top layer of the same system.

exchange pattern arises only in those layers that are at the interface with MgO. Figure 3(c) shows the top view of the DMI magnitude for the top layer, where a nontrivial relationship among the neighbors of both direction and magnitude of DMI can be seen, and, as they lie in the x-y plane, they can induce noncollinear spin configurations.

Using the spin model, we also investigate the effects of the anisotropy contributions on the overall effective value (see Fig. 4). The anisotropy is calculated using the constrained Monte Carlo method [25], an approach that allows

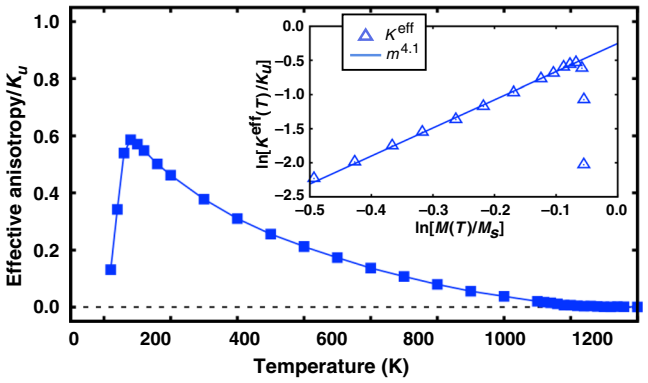

FIG. 4. Temperature dependence of the effective anisotropy as function of temperature for the $n_{\mathrm{Fe}} = 8$ system; lines provide a guide for the eye. The inset shows the scaling of the anisotropy with the total magnetization; the symbols represent the data; and the solid line the fit. The simulations are performed by first equilibrating the system for 10 000 Monte Carlo steps at each temperature and angle, and then the average of the torque is calculated over 50 000 steps.

one to constrain the direction of the magnetization away from the easy axis of the system. The anisotropy shows a surprising nonmonotonic behavior at low temperatures caused by the spin-spiral state. As the temperature-driven spin fluctuations increase, this destabilizes the spin-spiral ground state leading to an increase in the effective magnetic anisotropy as the magnetic ordering in the interface layer becomes more ferromagneticlike. Interestingly, the scaling of the effective magnetic anisotropy has an unusual exponent of $k(m)m^{4.1}$, which is expected for neither single-ion (m^3) or two-ion (m^2) anisotropy scaling. We attribute this unusual exponent to the frustrated nature of the exchange interactions at the interface, and so we expect a high exponent for the interface layer and lower for the subsurface layers, which when normalized to the average magnetization gives a higher effective scaling of the anisotropy constant.

IV. CONCLUSION

In conclusion, we present a fully relativistic electronic structure study of the exchange interactions and the site-resolved MAE of $\cdots \mathrm{MgO}/n_{\mathrm{Fe}}\mathrm{Fe}/\mathrm{MgO}\cdots$ $[n_{\mathrm{Fe}} = 4,\ 8]$ sandwiches. Our results reveal a dominant contribution to the MAE from the two-ion exchange anisotropy. Furthermore, we show that the competing ferromagnetic and antiferromagnetic interactions at the Fe/MgO interface lead to an overall ferromagnetic ground state but which includes a frustrated spin spiral at the interface, which destabilizes the magnetization of the interfacial layer at elevated temperatures, leading to a reduction of the Curie temperature of the system. The complex equilibrium magnetic properties of this technologically important material are of critical importance to understanding the thermal stability and spin-transport properties of nanoscale MTJ devices and can provide key insights into experimental observations.

ACKNOWLEDGMENTS

The financial support of the Samsung Global MRAM Innovation programme and the European Union under the Seventh Framework Programme under Grant No. 281043, FEMTOSPIN is gratefully acknowledged. ICN2 is supported by the Severo Ochoa program from Spanish MINECO (Grant No. SEV-2013-0295). R. C. also acknowledges the funding from the European Unions Horizon 2020 research and innovation program under the Marie Skłodowska-Curie Grant Agreement No. 665919. T. A. Ostler gratefully acknowledges the Marie Curie incoming BeIPD-COFUND fellowship program at the University of Liège. A. D., L. O., and L. S. acknowledge support by the Hungarian Scientific Research Fund (NKFIH) under Projects No. K115575, No. PD124380, No. K108676, No. K115608, and No. FK124723. L. O. also acknowledges to the National Quantum Technologies Program NKP-375 2017-00001 of the NRDI Office of Hungary. L. O. acknowledges support from the Janos Bolyai Scholarship of the Hungarian Academy of Sciences. L. S. and A. D. are grateful for financial support by the BME-Nanonotechnology FIKP grant of EMMI (BME FIKP-NAT).

[1] K. Mizunuma, S. Ikeda, J. H. Park, H. Yamamoto, H. Gan, K. Miura, H. Hasegawa, J. Hayakawa, F. Matsukura, and H. Ohno, MgO barrier-perpendicular magnetic tunnel junctions with CoFe/Pd multilayers and ferromagnetic insertion layers, Appl. Phys. Lett. **95**, 232516 (2009).

[2] J.-H. Park, C. Park, T. Jeong, M. T. Moneck, N. T. Nufer, and J.-G. Zhu, CoPt multilayer based magnetic tunnel junctions using perpendicular magnetic anisotropy, J. Appl. Phys. **103**, 07A917 (2008).

[3] G. Kim, Y. Sakuraba, M. Oogane, Y. Ando, and T. Miyazaki, Tunneling magnetoresistance of magnetic tunnel junctions using perpendicular magnetization $L1_0$-CoPt electrodes, Appl. Phys. Lett. **92**, 172502 (2008).

[4] L. Gao, X. Jiang, S.-H. Yang, J. D. Burton, E. Y. Tsymbal, and Stuart S. P. Parkin, Bias Voltage Dependence of Tunneling Anisotropic Magnetoresistance in Magnetic Tunnel Junctions with MgO and Al_2O_3 Tunnel Barriers, Phys. Rev. Lett. **99**, 226602 (2007).

[5] J. Stöhr and H. C. Siegmann, *Magnetism* (Springer, Berlin, 2006).

[6] I. Zutic, J. Fabian, and S. Das Sarma, Spintronics: Fundamentals and applications, Rev. Mod. Phys. **76**, 323 (2004).

[7] D. Weller, Y. Wu, J. Stohr, M. G. Samant, B. D. Hermsmeier, and C. Chappert, Orbital magnetic moments of Co in multilayers with perpendicular magnetic anisotropy, Phys. Rev. B **49**, 12888 (1994).

[8] C. J. Aas, P. J. Hasnip, R. Cuadrado, E. M. Plotnikova, L. Szunyogh, L. Udvardi, and R. W. Chantrell, Exchange coupling and magnetic anisotropy at Fe/FePt interfaces, Phys. Rev. B **88**, 174409 (2013).

[9] R. Cuadrado and R. W. Chantrell, Interface magnetic moments enhancement of FePt-L10/MgO(001): An ab initio study, Phys. Rev. B **89**, 094407 (2014).

[10] K. Nakamura, T. Akiyama, T. Ito, M. Weinert, and A. J. Freeman, Role of an interfacial FeO layer in the electric-field-driven switching of magnetocrystalline anisotropy at the Fe/MgO interface, Phys. Rev. B **81**, 220409(R) (2010).

[11] B. Rodmacq, S. Auffret, B. Dieny, S. Monso, and P. Boyer, Crossovers from in-plane to perpendicular anisotropy in magnetic tunnel junctions as a function of the barrier degree of oxidation, J. Appl. Phys. **93**, 7513 (2003).

[12] M. K. Niranjan, C.-G. Duan, S. S. Jaswal, and E. Y. Tsymbal, Electric field effect on magnetization at the Fe/MgO(001) interface, Appl. Phys. Lett. **96**, 222504 (2010).

[13] Kohji Nakamura, Yushi Ikeura, Toru Akiyama, and Tonomori Ito, Giant perpendicular magnetocrystalline anisotropy of 3d transition-metal thin films on MgO, J. Appl. Phys. **117**, 17C731 (2015).

[14] B. Yu. Yavorsky and I. Mertig, Noncollinear interface magnetism and ballistic transport in FeFeOMgOFe tunnel

junctions: Ab initio calculations using the KKR method, Phys. Rev. B **74**, 174402 (2006).
[15] B. Dupé, G. Bihlmayer, M. Böttcher, S. Blügel, and S. Heinze, Engineering Skyrmions in transition-metal multilayers for spintronics, Nat. Commun. **7**, 11779 (2016).
[16] S. Ikeda, K. Miura, H. Yamamoto, K. Mizunuma, H. D. Gan, M. Endo, S. Kanai, J. Hayakawa, F. Matsukura, and H. Ohno, A perpendicular-anisotropy CoFeB-MgO magnetic tunnel junction, Nat. Mater. **9**, 721 (2010).
[17] A. Hallal, H. X. Yang, B. Dieny, and M. Chshiev, Anatomy of perpendicular magnetic anisotropy in Fe/MgO magnetic tunnel junctions: First-principles insight, Phys. Rev. B **88**, 184423 (2013).
[18] N. Kazantseva, D. Hinzke, U. Nowak, R. W. Chantrell, U. Atxitia, and O. Chubykalo-Fesenko, Towards multiscale modeling of magnetic materials: Simulations of FePt, Phys. Rev. B **77**, 184428 (2008).
[19] J. M. Soler, E. Artacho, J. D. Gale, A. García, J. Junquera, P. Ordejón, and D. Sánchez-Portal, The SIESTA method for ab initio order-*N* materials simulation, J. Phys. Condens. Matter **14**, 2745 (2002).
[20] J. Zabloudi, R. Hammerling, L. Szunyogh, and P. Weinberger, *Electron Scattering in Solid Matter* (Springer, Berlin, 2005).
[21] See the Supplemental Material at http://link.aps.org/supplemental/10.1103/PhysRevApplied.9.054048 for details of the calculation procedures.
[22] L. Udvardi, L. Szunyogh, K. Palotás, and P. Weinberger, First-principles relativistic study of spin waves in thin magnetic films, Phys. Rev. B **68**, 104436 (2003).
[23] A. I. Liechtenstein, M. I. Katnelson, V. P. Antropov, and V. A. Gubanov, Local spin density functional approach to the theory of exchange interactions in ferromagnetic metals and alloys, J. Magn. Magn. Mater. **67**, 65 (1987).
[24] J. B. Staunton, L. Szunyogh, A. Buruzs, B. L. Gyorffy, S. Ostanin, and L. Udvardi, Temperature dependence of magnetic anisotropy: An ab initio approach, Phys. Rev. B **74**, 144411 (2006).
[25] P. Asselin, R. F. L. Evans, J. Barker, R. W. Chantrell, R. Yanes, O. Chubykalo-Fesenko, D. Hinzke, and U. Nowak, Constrained Monte Carlo method and calculation of the temperature dependence of magnetic anisotropy, Phys. Rev. B **82**, 054415 (2010).
[26] H. B. Callen and E. Callen, The present status of the temperature dependence of magnetocrystalline anisotropy, and the power law, J. Phys. Chem. Solids **27**, 1271 (1966).
[27] Jia Zhang, Christian Franz, Michael Czerner, and Christian Heiliger, Perpendicular magnetic anisotropy in CoFe/MgO/CoFe magnetic tunnel junctions by first-principles calculations, Phys. Rev. B **90**, 184409 (2014).
[28] R. F. L. Evans, W. J. Fan, P. Chureemart, T. A. Ostler, M. O. A. Ellis, and R. W. Chantrell, Atomistic spin model simulations of magnetic nanomaterials, J. Phys. Condens. Matter **26**, 103202 (2014).
[29] http://vampire.york.ac.uk.
[30] I. Dzyaloshinsky, A thermodynamic theory of weak ferromagnetism of antiferromagnetics, J. Phys. Chem. Solids **4**, 241 (1958).
[31] T. Moriya, Anisotropic superexchange interaction and weak ferromagnetism, Phys. Rev. **120**, 91 (1960).

Supplementary Material

I. Electronic Structure Methods

Structural Relaxation with SIESTA

The atomic structures were optimized by performing fully ionic conjugate gradient (CG) relaxation using the SIESTA package (2002 J. Phys.: Condens. Matter 14 2745). For the exchange-correlation potential we used the local spin density approximation (LSDA). We chose a common in–plane lattice constant found for optimized bulk MgO, specifically $a = 4{,}19$Å. The preferential adsorption site for the Fe atoms is above the O sites (R. Cuadrado and R. W. Chantrell, Phys. Rev. B **89**, 094407 (2014)), so we therefore construct a supercell consisting of 18 MgO + nFe + 18 MgO planes repeated periodically along the z coordinate, shown schematically in Supplementary Fig. 1. After the relaxation, the forces per atom were less than 0.02 eV/Å and the energy tolerance on each self–consistent cycle was less than 10^{-4}eV. Due to the in–plane mismatch between MgO and Fe bulk, the optimization process tends to change the out–of–plane distances with respect to the pure *bcc*–Fe phase leading to a body-centered tetragonal structure for the Fe.

During the optimization process the atomic out–of–plane Fe distances close to the interface developed minute asymmetries no more than ± 0.005Å. To avoid small deviations in any of the calculated magnetic properties we mirrored the out–of–plane distances with respect to the center of the Fe slice.

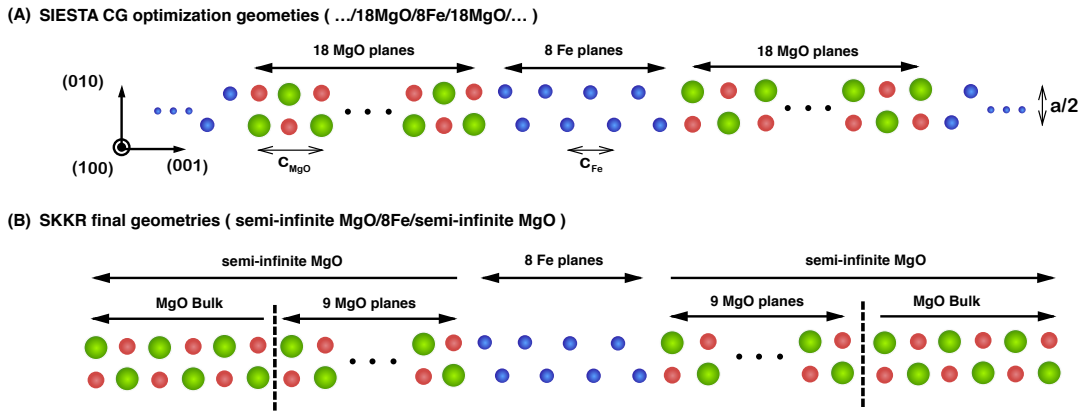

Figura 1: (A) Specific periodic geometry representation of 8 Fe layers sandwiched by 18 MgO planes used in the SIESTA optimization process. (B) Final geometry employed in the Wein/Budapest–SKKR code composed of the 8 Fe layers sandwiched by two semi–infinite MgO parts.

SKKR Calculations

For the SKKR calculations we also used the LSDA with Ceperley and Alder's parametrization (D. M. Ceperley and B. J. Alder, Phys. Rev. Lett. **45**, 566 (1980)) and the effective potentials and fields were treated within the atomic sphere approximation (ASA). All the SKKR calculations were carried out with the fully–relativistic Hamiltonian and the angular momentum cutoff was

set to l_{max}=2. A semicircular contour with 16 energy points was used for the necessary energy integrations.

For the calculation of the magnetic anisotropy energy we used the magnetic force theorem, where the total energy of the system can be replaced by the single–particle (band) energy. Employing the torque method (A.I. Liechtenstein, *et al*, J. Magn. Magn. Mater. **67**, 65 (1987)), in leading (second) order of the spin-orbit coupling, the uniaxial magneto-crystalline anisotropy constant, K, can be calculated as (see C. J. Aas, *et al* Phys. Rev. B **88**, 174409 (2013)):

$$K = E(\theta = 90^\circ) - E(\theta = 0^\circ) = \frac{dE}{d\theta}\Big|_{\theta=45^\circ} \tag{1}$$

where θ is the angle of the magnetization direction with respect to the [001] direction (i.e. perpendicular to the interface). Within the SKKR formalism, K can be decomposed into site–resolved contributions, K_i:

$$K = \sum_i K_i \tag{2}$$

Full details on the torque method can be found in J. B. Staunton *et al*, Phys. Rev. B **74**, 144411 (2006).

The $\mathcal{J}_{ij}$ matrices are less straightforward to calculate. The exchange tensor can be divided into three terms (L. Udvardi, *et al*, Phys. Rev. B **68**, 104436 (2003)):

$$\mathbf{S}_i \mathcal{J}_{ij} \mathbf{S}_j = J_{ij} \mathbf{S}_i \cdot \mathbf{S}_j + \mathbf{S}_i \mathcal{J}^S_{ij} \mathbf{S}_j + \mathbf{D}_{ij} \cdot (\mathbf{S}_i \times \mathbf{S}_j). \tag{3}$$

Here the first and second terms on the right hand side are the isotropic and symmetric anisotropic exchange interactions, respectively and the third term is the Dzyaloshinsky–Moriya (DM) interaction (T. Moriya, Phys. Rev. **120**, 91 (1960)), where the $\mathbf{D}_{ij}$ are defined as:

$$D^x_{ij} = \frac{1}{2}(J^{yz}_{ij} - J^{zy}_{ij}), \quad D^y_{ij} = \frac{1}{2}(J^{zx}_{ij} - J^{xz}_{ij}), \quad D^z_{ij} = \frac{1}{2}(J^{xy}_{ij} - J^{yx}_{ij}) \tag{4}$$

The components of the exchange tensor, $\mathcal{J}_{ij}$ can be conveniently found by taking second derivatives of the Hamiltonian with respect to polar and azimuthal angles of the spins:

$$\frac{\partial^2 \mathcal{H}}{\partial \alpha_i \partial \beta_k} = \delta_{ik} K^{\alpha\beta}(\mathbf{S}_i) + \delta_{ik} \sum_{j(\neq i)} \mathbf{S}^{\alpha\beta}_i \mathcal{J}_{ij} \mathbf{S}_j + (1 - \delta_{ik}) \mathbf{S}^{\alpha}_i \mathcal{J}_{ik} \mathbf{S}^{\beta}_k \tag{5}$$

where α or β can be either θ or ϕ (polar and azimuthal angles respectively) and

$$K^{\alpha\beta}(\mathbf{S}_i) = \frac{\partial^2 K(\mathbf{S}_i)}{\partial \alpha_i \partial \beta_i}, \quad \mathbf{S}^{\alpha}_i = \frac{\partial \mathbf{S}_i}{\partial \alpha_i}, \quad \mathbf{S}^{\alpha\beta}_i = \frac{\partial^2 \mathbf{S}_i}{\partial \alpha_i \partial \beta_i} \tag{6}$$

As was shown in L. Udvardi, *et al*, Phys. Rev. B **68**, 104436 (2003), the full exchange matrix and anisotropy contributions can be obtained by taking combinations of the derivatives of the Hamiltonian with respect to the angles and constraining the magnetization along different reference orientations,through integration over the scattering path operators to the Fermi energy (see L. Udvardi, *et al* for full details). The full exchange tensor was calculated up to a maximum number of three times the in-plane lattice constant for all the n_{Fe} thicknesses.

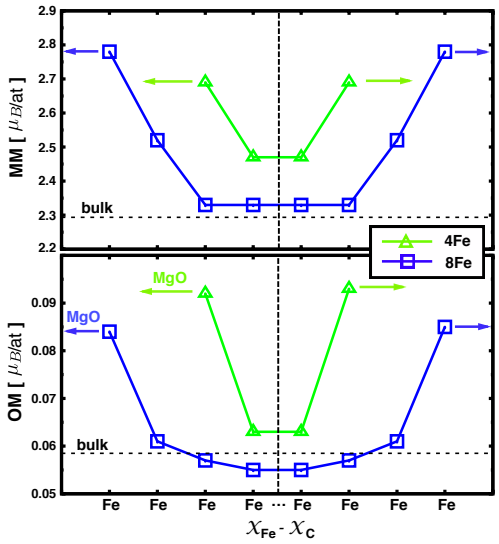

Figura 2: Layered resolved magnetic and orbital moments for different sandwiched Fe thicknesses by MgO alloy, up and down graphs, respectively. Vertical black dashed line represents the center of each geometric configuration and the coloured arrows the begining of the Fe/MgO interface. Horizontal dashed lines depict magnetic and orbital moment values of *bcc*–bulk Fe. $\mathcal{X}_C$ represents the center of each geometric configuration.

II. Variation of the localized magnetic moments

In the figure 2 are shown the Fe site resolved magnetic (MM) and orbital moment (OM) values of the $\cdots$MgO/n_{Fe}Fe/MgO$\cdots$ [n_{Fe}=4,8] structures, up and down graphs, respectively. The Fe MM at the interface tends to increase its values up to around 2.8μ_B for the two configurations, reducing it inwards into the center of the sandwich which value has reduced in $\sim$0.5μ_B. This trending is quite fast since that the third plane has almost achieved the *bcc*–Fe bulk MM value of 2.3μ_B. As well as the thickness of the Fe slice increases the MM at the center decreases too, having the bigger value for n_{Fe}=4. On the other hand, the MM values at the edges are only a bit dependent with Fe thickness, having almost the same value. The enhancement of the MM at the interface are mainly due to the changes in the unit cell shape after the optimization process that guides the Fe atoms to an out–of–plane tetragonality and in addition due to the increment in the unbalance between the up and down states. The OM are strongly affected by the interface in a similar way that the MM, albeit for different thicknesses, the values at the interfaces are different, having higher contribution for the smaller Fe slice size and decreasing for the bigger one.

III. Equilibrium Magnetization

The layer–resolved temperature dependence of the magnetization, calculated using the spin model, is shown in Fig. 3. Compared to bulk bct and bcc Fe (M. Ležaić, *et al*, Appl. Phys. Lett. **90**, 082504 (2007)) we find a significantly reduced Curie temperature owing to the small size of the system and the presence of strong in–plane antiferromagnetic interactions. The temperature dependence of the other layers in the system are remarkably similar, showing the highly localized nature of the magnetic interactions induced by the MgO.

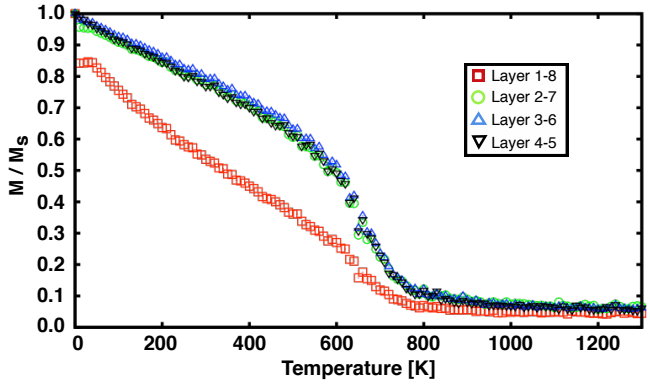

Figura 3: Simulated layer–resolved temperature dependent magnetization for the $n_{Fe} = 8$ system. The Fe/MgO interface layer shows a reduced low temperature ordering due to the spin spiral state, and much stronger temperature dependence of the magnetization due to spin frustration. The results are obtained equilibrating the system for 10000 Monte Carlo steps and averaging over 50000 steps.

IV. Temperature dependence of spin spiral

Fig. 3 shows a ground state for $n_{Fe} = 8$ characterized by an interfacial non-collinear configuration that is caused by the peculiar exchange coupling in these layers. Fig. 4 presents snapshots of the magnetic configurations for the top four layers of the $n_{Fe} = 8$ system at different temperatures. A different magnetic ordering between the top–interfacial layer and the other Fe layers can be observed at 25 K even though spin fluctuations due thermal agitation are found. Snapshots

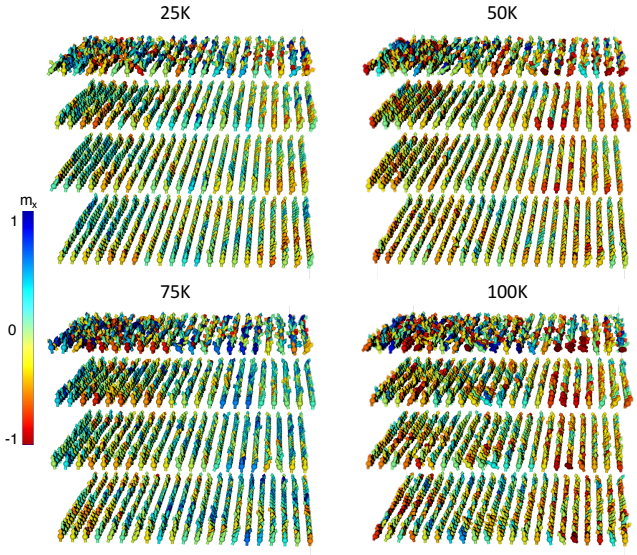

Figura 4: Snapshots of the spin configuration showing the temperature evolution of the spin spiral for first 4 layers of the $n_{Fe} = 8$ system. The non-collinear character starts being lost as the thermal contribution increases and is lost at $T = 50$ K. The color scheme describes the x-component of the magnetization (blue for $+x$, red for $-x$ and green for $x = 0$).

obtained at higher temperature show the loss of this feature and a more uniform layer behavior emerges. This re-orientation of the spin structure in visible in the temperature of the magnetization presented in Fig. 3 where the magnetization is constant until 50 K and recovers a decreasing trend for higher temperatures. Similarly, the temperature dependence of the effective anisotropy changes drastically around 50 K, exhibiting a transition from increasing (< 50 K) to decreasing (> 50 K).